

Division - Soil Processes and Properties | Commission - Soil Physics

Automatic measurement of water infiltration into the soil

Lucas Raimundo Rauber^{(1)*} , Micael Stolben Mallman⁽¹⁾ ,
Dalvan José Reinert⁽¹⁾ , Fábio Soares Pires⁽²⁾ , Francieli de Vargas⁽¹⁾  and
Paulo Ivonir Gubiani⁽¹⁾ 

⁽¹⁾ Universidade Federal de Santa Maria, Departamento de Solos, Santa Maria, Rio Grande do Sul, Brasil.

⁽²⁾ Universidade Federal de Santa Maria, Departamento de Engenharia Agrícola, Santa Maria, Rio Grande do Sul, Brasil.

ABSTRACT: In hydrological modeling and for the development of projects related to soil and water conservation and civil engineering, determination of water infiltration variables into the soil plays a key role. However, measuring infiltration with manual infiltrometers is work-intensive and requires several people, which casts doubts on the consistency of the process description. Our objective was to develop automated and compact systems for data acquisition by double-concentric-ring and Cornell infiltrometers. The systems are based on air differential pressure sensors and microcontrollers using open-source software and a simple construction. We developed ten sets of automatic infiltrometers for each method that were properly calibrated. The equipment was validated in the field, and the alignment of the automatically measured with the hand-measured infiltration data was considered satisfactory. The proposed systems make data records of infiltration and associated variables possible, with less operator dependence than manual measurement strategies. In addition, the enhanced resolution resulting from infiltrometer automation makes the infiltration curve more representative, especially in the initial infiltration stage.

Keywords: ring infiltrometer, Cornell infiltrometer, microcontroller, Arduino software.

* **Corresponding author:**
E-mail: lucas.rauber@ufsc.br

Received: July 02, 2023

Approved: November 20, 2023

How to cite: Rauber LR, Mallman MS, Reinert DJ, Pires FS, Vargas F, Gubiani PI. Automatic measurement of water infiltration into the soil. Rev Bras Cienc Solo. 2024;48:e0230078
<https://doi.org/10.36783/18069657rbc20230078>

Editors: José Miguel Reichert  and Cássio Antônio Tormena .

Copyright: This is an open-access article distributed under the terms of the Creative Commons Attribution License, which permits unrestricted use, distribution, and reproduction in any medium, provided that the original author and source are credited.



INTRODUCTION

Water infiltration into the soil is generally the main hydrological process that compartmentalizes rain or water applied to the soil. Therefore, the infiltration variables, such as cumulative infiltration and steady infiltration rate (SIR), are key to hydrological modeling, water and soil conservation planning, and sizing of irrigation systems and civil engineering projects (Assouline, 2013). For example, cumulative infiltration data are the basis for an adequate design of hydraulic installations to contain surface runoff, such as level terraces. The steady infiltration rate underlies the definition of maximum water application rate in irrigation systems and in sizing hydraulic constructions to regulate surface runoff. In addition, SIR is used for appropriate planning of wastewater disposal sinks, according to the technical norm No. 05/2017 (Fepam, 2019).

Due to the high spatial variability of point infiltration, a large number of measurements would be necessary to collect representative infiltration data of an area. In different fields of knowledge, this situation challenges the operational capacity of researchers and technicians (Morbidelli et al., 2018; Lewis et al., 2021). Moreover, the measurements must be done by hand, usually with ring or disc infiltrometers (Rahmati et al., 2018), which is a laborious procedure for which more than one person is required. In this sense, measurement automation has been proposed and tested. For example, systems with pressure transducers are one of the main means of automating infiltration reading (Arriaga et al., 2010; Moret-Fernández et al., 2012; Di Prima, 2015; Di Prima et al., 2016; Fatehnia et al., 2016; Cernicchiaro et al., 2019; Abdelmoneim et al., 2021), since the principle of most methods is the measurement of variation of a hydraulic load over time. Hydraulic load monitoring can also be done with a smartphone camera (Latorre et al., 2021). Another way of evaluating infiltration automatically is with a tipping-bucket gauge to monitor runoff and precipitation (Somavilla et al., 2019).

Most of the above automation systems proposed so far have been tested with ring or disc infiltrometers, while the automation of Cornell infiltrometer, a portable rain simulator, was less investigated (Ogden et al., 1997; van Es and Schindelbeck, 2003; Seratto et al., 2019). Moreover, simpler and more compact automation systems associated with low-cost and open-source microcontrollers should be more extensively tested to make infiltration measurement process even more practical. Our objective was to develop and validate compact automation systems to acquire point water infiltration data with double-concentric-ring and Cornell infiltrometers.

MATERIALS AND METHODS

Reading systems

The systems consisted of differential air pressure sensors connected to a microcontroller to monitor infiltration. These sensors are widely used for hydraulic load monitoring by reading air pressure or suction and subsequently correlating the results with hydraulic load. This principle applies to infiltrometers because point infiltration involves the discharge of water from tanks or reservoirs, in which hydraulic load can be monitored with differential pressure sensors and, subsequently, the amount of water that infiltrates into the soil can be calculated.

Sensors had two holes - one for vacuum and the other for positive pressure (> atmospheric). For the ring infiltrometer, MPX5010DP differential pressure sensors (NXP Freescale Semiconductors) were used (Figure 1), which have an operating limit of up to a differential pressure of a 100 cm water column. Two pressure sensors NPX MPXV4006DP were used for the Cornell infiltrometer (Figure 2), at an operating limit of a 60 cm water column. Characteristics of each infiltrometer can explain this difference in the operating threshold between the methods. The same volume of infiltrated water causes a smaller decrease

in the water column of the Cornell infiltrometer than in the water column of the ring infiltrometer. Consequently, sensors with a higher resolution are required for the Cornell infiltrometer to ensure accuracy in measurements similar to that of both infiltrometers.

For both infiltrometers, ten sets of automated systems were developed (infiltrometer with automatic reading system). For each set, a system with a switch, microcontroller, SD card for data storage, and capacitors (further details in Figures 1 and 2) was placed in a plastic box (29 × 42 × 82 mm); only the sensors and the 12 V battery were attached on the outside of the box. It is worth mentioning, however, that there is enough additional space inside the box to include a 9V battery if the 12V battery and the power cabling from the battery to the microcontroller are not wanted. Details of the components and connections are shown in figures 1 and 2. Systems were programmed to record the pressure differential every second.

Installation of sensors in infiltrometers

In infiltration measurements with double concentric rings, the height of the above-ground water column may be variable or constant (Bouwer, 1986). We proposed an automatic reading system for constant load. Initially, Mariotte columns with PVC tubes (diameter 10 cm, height 100 cm) were installed (Figure 3). Plugs and flange-type adapters with a PVC ring were attached to the upper and lower parts of these tubes and coupled with ball valves (1/4") (Figure 3). An opening of approximately 10 mm was cut in the upper part of each tube to fix the differential pressure sensor that reads the suction (Figure 3); through the vacuum hole, the sensor is in contact with the internal air suction under the water column in the infiltrometer, while the second hole is exposed to external atmospheric pressure. Externally, a transparent hose was also attached to each PVC tube to connect the tube's upper and lower internal parts and make visual monitoring of the water level variation within the tube possible. Metal tripods were used to fix the PVC pipes beneath the ground (Figure 3).

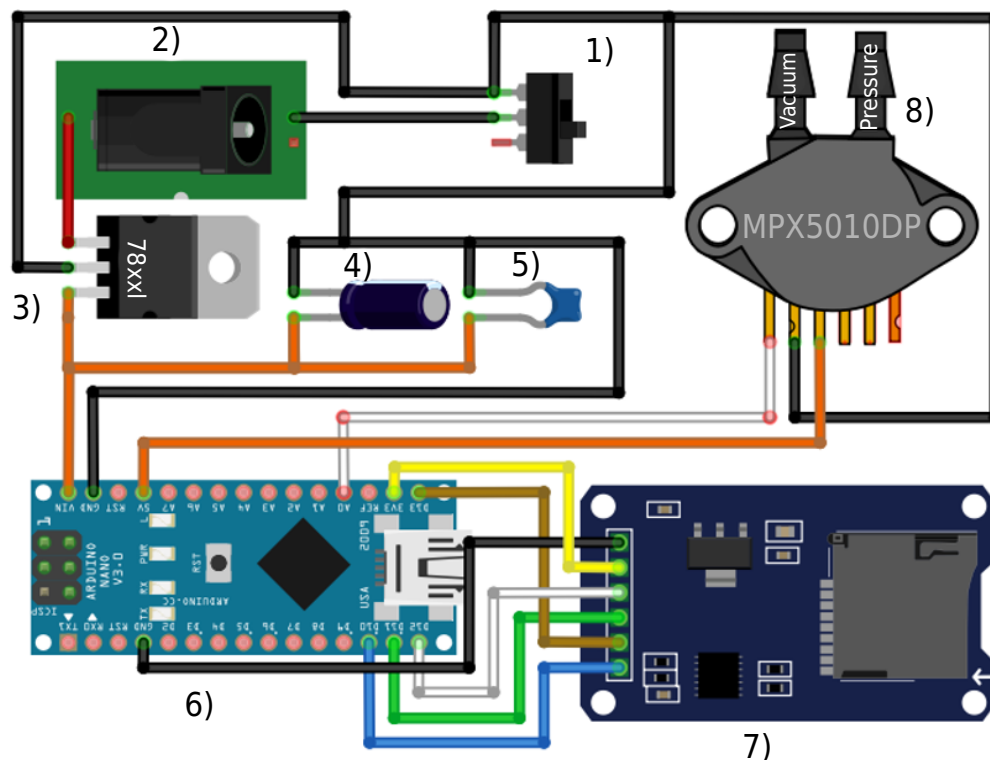


Figure 1. Automatic system scheme for obtaining data to evaluate soil water infiltration with a double concentric ring method. (1) switch; (2) plug for power input (12 V); (3) voltage regulator (7809); (4 and 5) capacitors; (6) microcontroller; (7) SD card module; and (8) air differential pressure sensor (MPX5010DP).

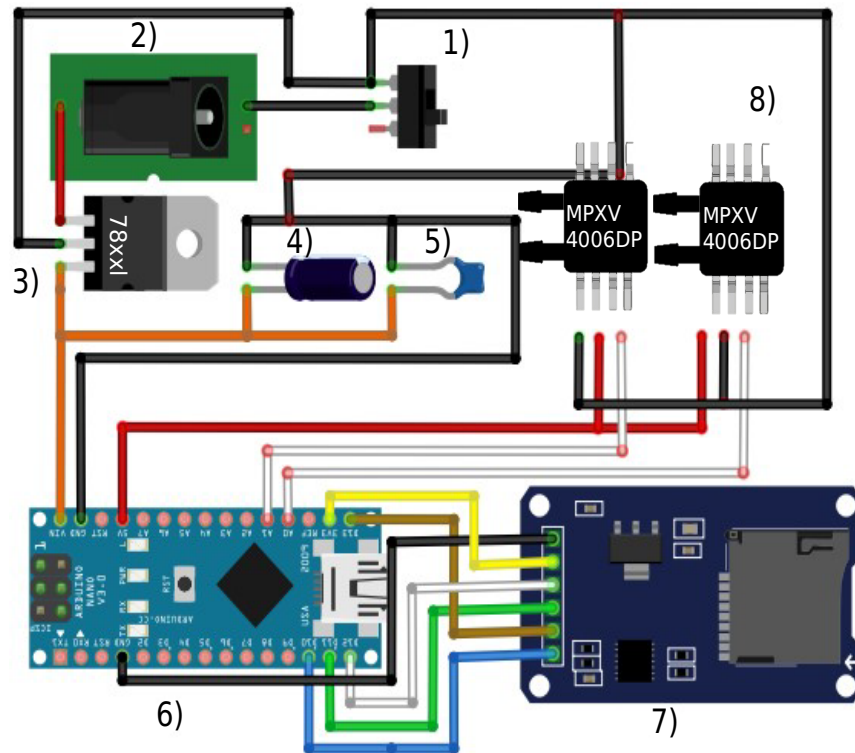


Figure 2. Automatic data collection system to evaluate soil water infiltration with a Cornell infiltrometer (portable precipitation simulator). (1) switch; (2) plug for power input (12 V); (3) voltage regulator (7809); (4 and 5) capacitors; (6) microcontroller; (7) SD card module; and (8) air differential pressure sensors (MPXV4006DP).

The principle of measuring apparent water infiltration with the Cornell infiltrometer is based on the difference between precipitation and surface runoff (Ogden et al., 1997; van Es and Schindelbeck, 2003; Seratto et al., 2019). The infiltrometer is coupled to a ring inserted into the soil and generates artificial precipitation on the soil within the ring (Figure 4). A hole on the side of the ring conducts surface runoff to a reservoir; the difference between the water column of the infiltrometer and runoff volume is generally determined every three min to compute the precipitation and accumulation, surface runoff, and infiltration rates (Seratto et al., 2019).

Construction and adaptation of the Cornell infiltrometers in this study were based on the initially proposed method model (Ogden et al., 1997; van Es and Schindelbeck, 2003), with some modifications (Seratto et al., 2019). For each infiltrometer, an acrylic tube (diameter 25 cm, height 50 cm) was initially sealed at the ends with polypropylene plates (Figure 4). In the lower plate, 112 microtubules (diameter 0.06 cm, length 20 cm) were inserted, which were siphoned to cause water dripping during the tests. At the upper end, the infiltrometer has two holes (Figure 4). A glass capillary tube is attached to one of them and inserted into a sealing stopper, through which air enters the infiltrometer and maintains the intensity of precipitation constant, based on the Mariotte principle. Precipitation intensity can be varied by adjusting the depth of the submerged end of the capillary tube. The other hole serves to supply water. For the manual method, this hole is sealed with a stopper to prevent air from entering during the test. For automated measurements, however, a hole of approximately 10 mm was made in the stopper to insert a second capillary tube. By means of this tube, a differential pressure sensor (MPXV4006DP) to read air suction was coupled to the infiltrometer and connected with the vacuum orifice at the upper end of the second capillary tube (Figure 4).

To automate the surface runoff readings of the Cornell infiltrometer, a sensor (NXP Semiconductor MPXV4006DP) was installed directly in the runoff collection tank. This reservoir was installed in a trench, at a distance of 1.5 m from the infiltration ring (Figure 4). A hose attached to the ring with a plug carried the water to the reservoir,



Figure 3. General aspects of the constructed double concentric ring infiltrometer and the coupling of the system to automatically obtain infiltration data. (1) box with microcontroller and differential pressure sensor (MPX5010DP); (2) opening for water supply, with stopper-type lid for sealing; (3) PVC column that supplies water to the inner ring; (4) transparent hose for manual water level checking; (5) support tripod; (6) flange type adapter with ball valve for water outlet; (7) 12 V battery; (8) 2-way cable for power supply; (9) inner ring; and (10) outer ring.

maintained below the level of the water outlet hole in the ring. The reservoir capacity for this study was 20 L, near the maximum capacity of the Cornell infiltrometer. Thus, the equipment can monitor all surface runoff generated in tests, even in cases with infiltration close to zero. The flow measurement sensor was coupled to a glass capillary tube inserted vertically within the runoff collection tank. This capillary tube is initially immersed vertically in a water-filled test tube, and the upper end of the tube is then connected to the vacuum hole of the sensor. At this point, the capillary/sensor assembly is transferred to the runoff collection tank (Figure 4). This procedure was proposed for suction measurements, since we observed that it provided better sealing of the contact surface between the sensor and the capillary tube than positive air pressure.

Sensor calibration

Microcontrollers transformed the differential air pressure measured by the sensors into a scale of 0 to 4064 mV and recorded the results on an SD card at each pre-determined time. Subsequently, calibration curves were used to transform the sensor readings into water flow.

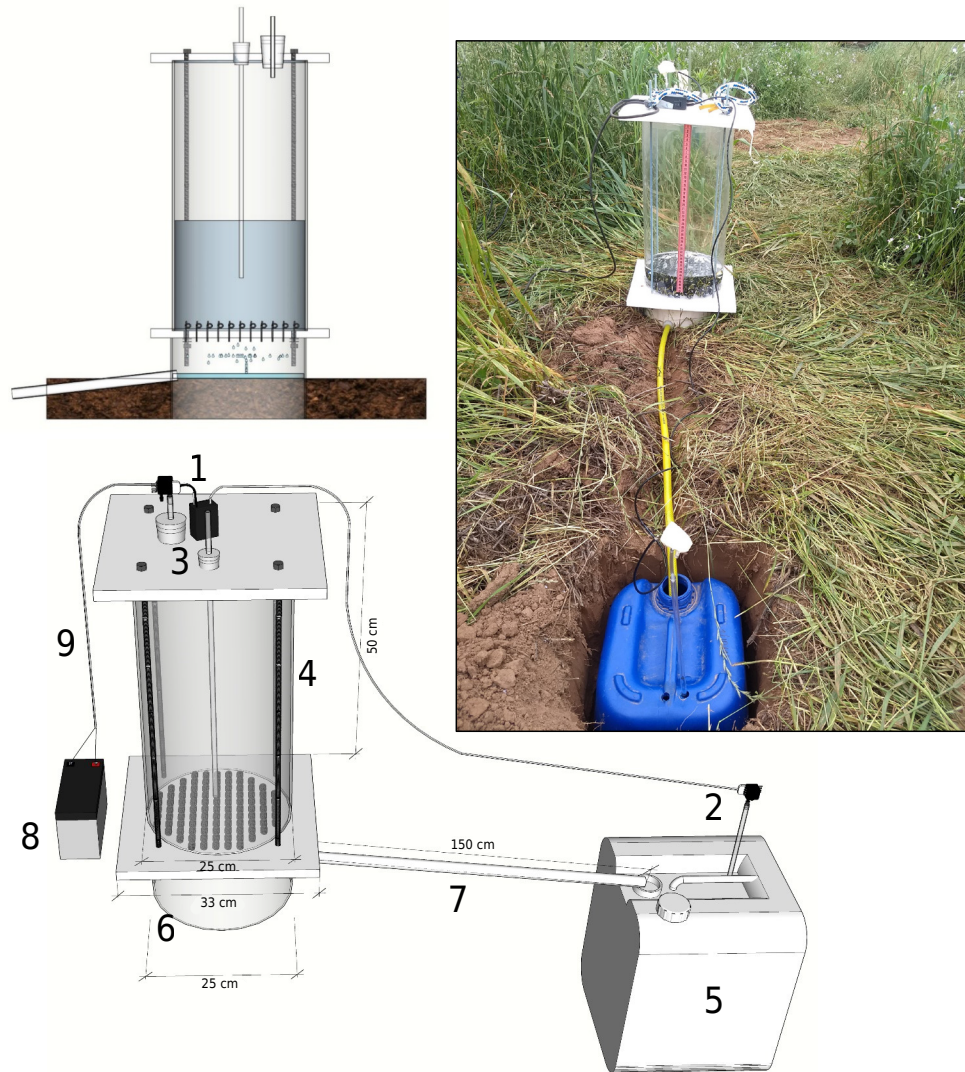


Figure 4. General aspects of the constructed Cornell infiltrometer and system coupling to automatically obtain infiltration data. (1) box with microcontroller where two differential pressure sensors (MPXV4006DP) are connected, the first being coupled to the infiltrometer for monitoring precipitation and the second (2) located under a glass capillary inserted vertically in the flow sampling container; (3) glass capillary that allows water to enter the equipment, which, under the Mariotte principle, maintains a constant precipitation rate; (4) Cornell water reservoir; (5) reservoir to accumulate surface runoff; (6) infiltration ring; (7) hose to conduct surface runoff; (8) 12 V battery; (9) power supply cable.

Each sensor was calibrated separately. To this end, the height of a water column at rest within a surface-sealed tank was altered step-wise, with subsequent manual recording of the hydraulic load or water volume and the values recorded by the sensors at each step (interval) of change in the hydraulic load. For real-time monitoring of sensor readings, we used open-source software Arduino IDE. In this case, the systems with microcontrollers and sensors were connected directly to a notebook.

The ring infiltrometer was calibrated directly within the device. Firstly, each PVC tube was completely filled with water. Without opening the upper valve, the sensor was attached to the infiltrometer. Subsequently, the water level within the infiltrometer was gradually lowered. At each discharge step (interval), the height of the water column was read manually on graduated rulers fixed externally to the infiltrometer, and the system recorded the sensor readings. Subsequently, only sensor readings after reaching stability were considered, i.e., when the water column came to rest after each step of lowering the hydraulic load. Finally, a linear equation was fitted between the readings recorded by the system (mV) and the height of the water column read manually on the infiltrometer. From the calibration straight line, the angular coefficient (cm mV^{-1}), which represents the reading resolution of the system, was extracted.

To calibrate the precipitation sensors of the Cornell infiltrometer, we followed the same principle as for the ring infiltrometer. However, in this case, the sensors were attached to the external end of a glass capillary tube inserted vertically inside a transparent test tube; a graduated ruler was attached to the outside of the capillary tube. The tube was initially immersed vertically in a test tube filled with water and then coupled to the vacuum orifice of the sensor at the upper end of the capillary. Then, the capillary tube with the sensor was removed from the water-filled test tube and placed vertically in a second test tube. Initially, this one contained no water, and the calibration procedure was carried out on it; for this sensor, we also observed that under suction, sealing at the sensor/capillary contact is better than positive air pressure. Thus, water was gradually added into the test tube; at each step of change in hydraulic load, the position of the water in the test cylinder was manually read and the automatic system recorded the values. Finally, the angular coefficient of the linear fitting was computed.

Surface runoff reading sensors in the Cornell infiltrometer were calibrated directly in the runoff collection tanks. Because these tanks are not shaped geometrically as cylinders or cubes, monitoring the water height in the tanks would not allow an accurate calculation of the drained water volume. Therefore, calibration was based on the relationship between the cumulative water volume in the tank (mL) and readings of the pressure sensors (mV). In this way, at each calibration step, the water volume added to the tank was measured in a graduated cylinder, and the automatic system recorded the corresponding suction value. Sensor was attached to the external end of a glass capillary tube placed vertically in the tank (Figure 4). However, this capillary tube had previously been immersed in a test tube filled with water and subsequently coupled to the vacuum hole of the sensor at the upper end of the capillary tube. Only then was the capillary/sensor assembly linked to the tank to operate in suction mode, as did the other sensors. Finally, a quadratic model was fitted between cumulative volume (mL) and system recording units (mV).

Infiltration measurement in the field with automated infiltrometers

Numerous field infiltration tests were carried out with both types of automated infiltration meters. Significant oscillations in sensor readings were observed for the ring infiltrometer, when water was discharged and air entered the PVC column (Figure 5), which caused relief of the hydraulic load and suction within the PVC column. As the water level rose within the inner ring, air entry into the PVC column was interrupted, which also interrupted the water outlet. Nevertheless, the internal hydraulic load (at the base) and suction (at the top) were quickly stabilized and correctly read by the sensors. Therefore, the readings of the moments of water discharge and air entry were removed to maintain the readings of interest (represented by red dots in Figure 5). Since the time for stabilization of the readings after each water discharge is of the order of 5 to 10 s, a high reading frequency is necessary to clearly distinguish the atypical points to be removed (Figure 5). Atypical points were detected and removed using Excel VBA algorithm, a procedure similar to that proposed by Di Prima (2015). After defining the points of interest, the infiltration rate for each discharge interval was calculated with equation 1, whose integral represents the cumulative infiltration.

$$i \text{ double ring} = \left[\frac{a(X_{n+1} - X_n)}{t_{n+1} - t_n} \right] \times \frac{Ab1}{Ab2} \quad \text{Eq. 1}$$

in which: i is the infiltration rate (cm h^{-1}); a is the calibration angular coefficient (cm mV^{-1}); X_n and X_{n+1} are the sensor readings (mV) at times t_n and t_{n+1} (h), respectively; $Ab1$ is the internal base area of the infiltrometer PVC tube (cm^2); and $Ab2$ is the base area of the internal ring inserted into the soil (cm^2).

For the Cornell infiltrometer, the differential pressure sensors provided no atypical readings, neither in the infiltrometer nor in the runoff collection tank (Figure 6). This possibly occurred because the water column in both reservoirs is not affected by abrupt oscillations. Thus, the points of interest can be delimited without prior data processing. Nevertheless, a high frequency of data recording seems desirable, so that the values

can be averaged for each interval of interest, and any error arising from the natural fluctuation of the values recorded by the system can consequently be minimized (Figure 6). Precipitation intensity ($prec$) at each time interval can be calculated by equation 2 and the runoff rate by equation 3. Finally, the infiltration rate is computed as the difference between instantaneous precipitation and surface runoff (Equation 4). The time to ponding can easily be detected by the Cornell infiltrometer methodology, as the moment when the pattern of the values recorded by the runoff sensor after the start of the test begins to change (Figure 6). The time to ponding represents the period elapsed from the beginning of precipitation until runoff sets in or is properly detected by the reading system (Figure 6). Cumulative precipitation until ponding represents the initial abstraction, a variable also used in hydrological models. Cumulative precipitation, surface runoff and infiltration are calculated by integrating equations 2, 3 and 4, respectively.

$$prec = \left[\frac{a(X_{n+1} - X_n)}{t_{n+1} - t_n} \right] \times \frac{Ab3}{Ab4} \quad \text{Eq. 2}$$

$$esc = \left[\frac{V(X_{n+1}) - V(X_n)}{t_{n+1} - t_n} \right] / Ab4 \quad \text{Eq. 3}$$

$$i_{cornell} = prec - esc \quad \text{Eq. 4}$$

in which: $prec$ is the instantaneous precipitation (cm h^{-1}); X_n and X_{n+1} are the readings of the precipitation sensors (mV) at times t_n and t_{n+1} (h); a is the angular coefficient (cm mV^{-1}); $Ab3$ is the internal base area of the Cornell infiltrometer (cm^2); $Ab4$ is the internal base area of the ring inserted into the soil (cm^2); $V(X_n)$ and $V(X_{n+1})$ are the cumulative water volumes (mL) obtained by the calibration equation for points X_n and X_{n+1} at times t_n and t_{n+1} (h); esc is the instantaneous surface runoff (cm h^{-1}); and i is the infiltration rate (cm h^{-1}).

Validation

For the validation phase, we analyzed the relationship between the infiltration variables evaluated by the automated sets and manual evaluation. Both automated and manual assessments were carried out on the same equipment simultaneously, since the equipment allows both forms of reading. Validation was carried out on an *Argissolo Vermelho-Amarelo Distrófico abruptico* (Table 1) (Santos et al., 2018) – Ultisol (Soil Survey Staff, 2014) –, in Santa Maria, Rio Grande do Sul, in an area under long-term no-tillage management (~20 years) and another no-tillage area with subsoiling ($29^\circ 43' 11''$ S $53^\circ 42' 12''$ W). These two management forms were used to expand the range of infiltration values. For example, significantly greater infiltration is expected in the subsoiled area. We used ten sets of infiltrometers for each method for automatic and manual evaluations under both managements. The infiltration measurement points were spaced 3 to 6 m apart for each management and method, and the systems were powered with a 12 V (45 Ah) battery. Variables of interest were cumulative infiltration and steady infiltration rate, measured with the double-ring infiltrometer, as well as the precipitation rate, cumulative surface runoff and infiltration and steady infiltration rates, obtained with the Cornell infiltrometer.

For the double-concentric ring infiltrometer, 2-hour tests were carried out at each point. Manual readings were performed every 2 min at the beginning (up to 10 min) and then every 10 min until the end of the test. The hydraulic load was constant at 3 cm. For the Cornell infiltrometer, the tests lasted approximately 1 h; the exact test duration was related to the precipitation intensity applied since the infiltrometer was not replenished to avoid interrupting the test. Most commonly, a precipitation intensity of 300 mm h^{-1} is used (Seratto et al., 2019), but intensities between 168 and 476 mm h^{-1} were used here, to evaluate whether the accuracy of the systems would be affected by the precipitation rate. Cumulative precipitation and surface runoff were read manually every 3 min.

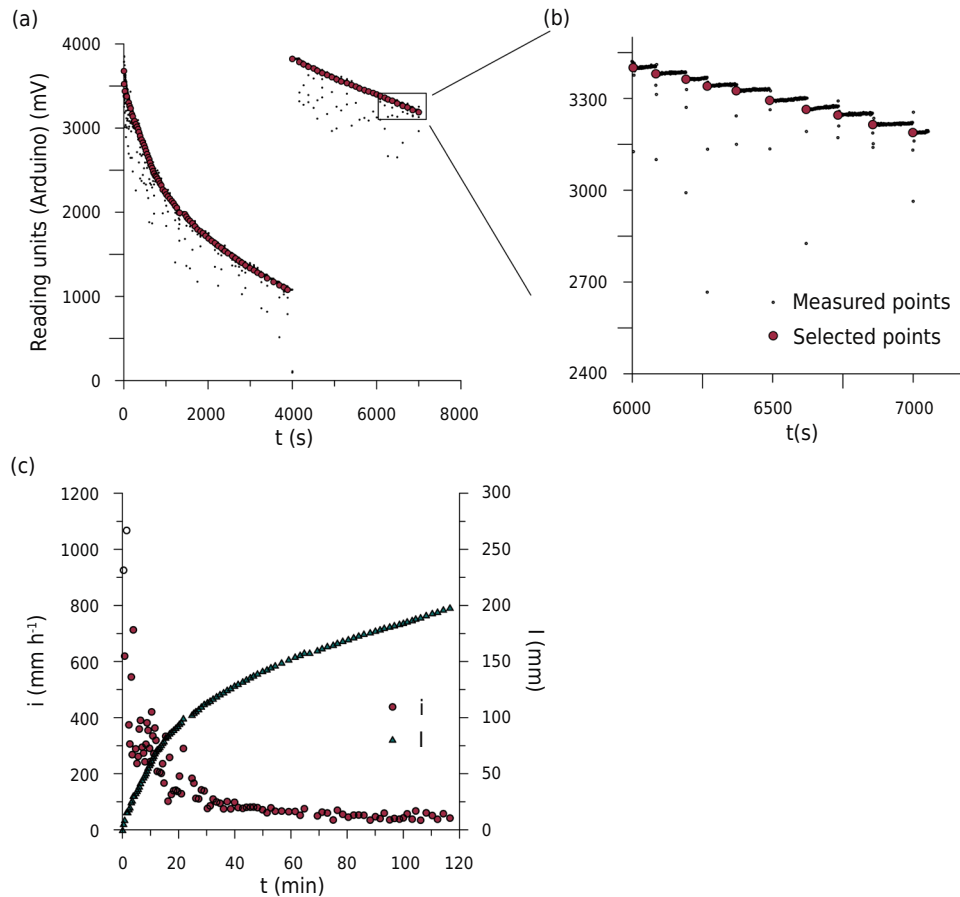


Figure 5. Data obtained by an automated double-ring infiltrometer. Data recorded by the sensor (a). Enlarged scale to facilitate visualization of the selected points (in red) (b); corresponding infiltration rate (i) calculated with equation 1 and its integration resulting in accumulated infiltration (I) (c).

Statistical analysis

Quality of the calibration stage fittings was assessed by residual analysis. The Shapiro-Wilk (normality distribution), Durbin Watson (independence) and Breusch-Pagan (homogeneity of variance) tests were performed in the R environment, considering an error probability of 5 %. In addition, the accuracy of fittings was analyzed through the root-mean-squared error (RMSE).

Accuracy of the methods to be validated was evaluated by the RMSE, Nash-Sutcliffe efficiency model (NSE), Willmott agreement index (Willmott) and Percent Bias (Pbias). Manual and automatic readings were compared with regard to the variables steady infiltration rate and cumulative infiltration (for both methods) and also the RMSE, NSE, Willmott and Pbias of precipitation rate, steady state infiltration rate, and accumulated surface runoff and infiltration for the Cornell infiltrometer. Furthermore, a linear equation was fitted to manual and automatic reading for each variable, with due error analysis.

RESULTS AND DISCUSSION

Angular coefficient and statistics of fitting and error analysis for each sensor evaluated in the calibration stage are listed in tables 2 to 4. The mean angular coefficient was $0.0274 \text{ cm mV}^{-1}$ for the double-ringed and $0.0161 \text{ cm mV}^{-1}$ for the Cornell sprinkle infiltrometer. For these fittings, the errors were normal, independent, with homogeneous variance, which indicates satisfactory linearity of fitting and ability to transform sensor readings

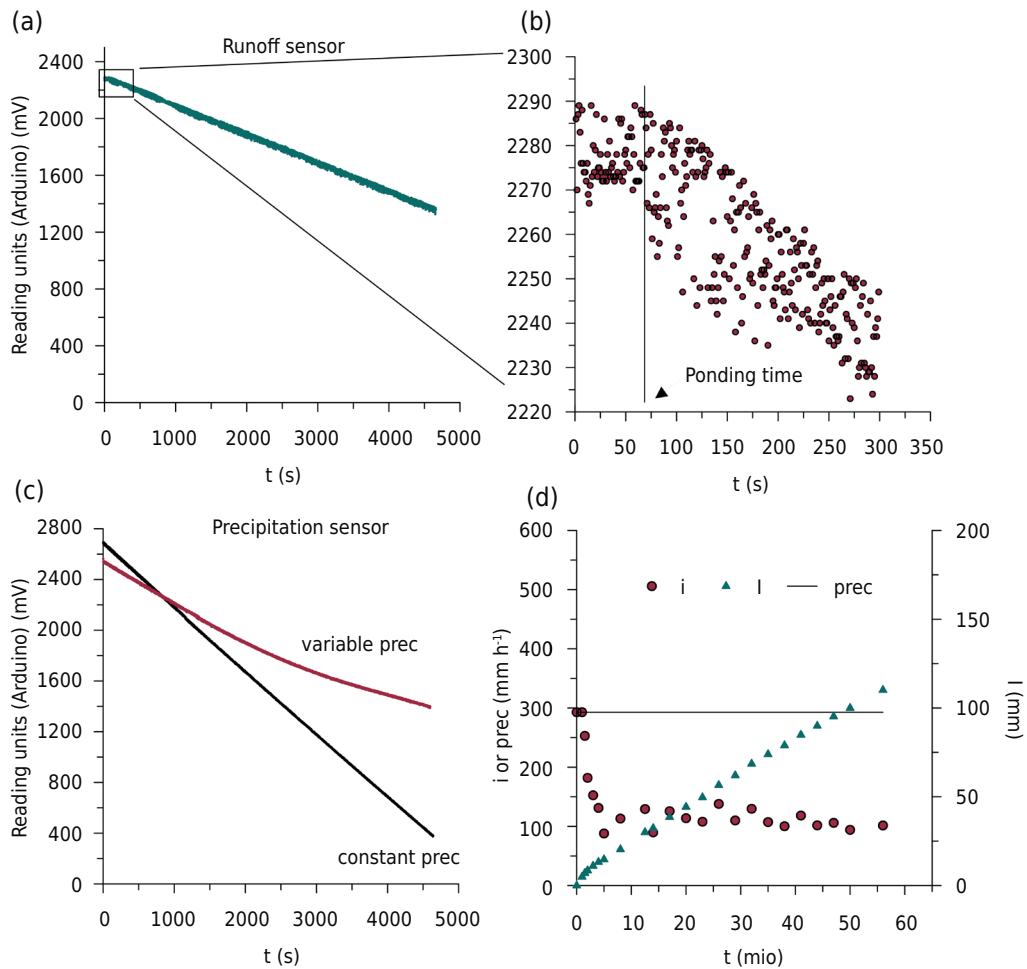


Figure 6. Experimental data from an automated system with a Cornell infiltrometer. Records obtained by the runoff sensor (a). Enlarged scale in figure 6b to detect the time for ponding (time elapsed from the beginning of precipitation until surface runoff begins); (c) precipitation sensor records over time, demonstrating (i) condition with linearity in the suction trend over time and, therefore, constant precipitation intensity (prec) and (ii) condition with non-linearity of suction over time, indicating precipitation intensity variable; (d) infiltration variables obtained, where “i” is the infiltration rate and “I” is the accumulated infiltration.

into water flow throughout the measurement range of the microcontroller (0-4064 mV). A small difference in the angular coefficient was also observed between the sets assembled for the same method (Tables 2 and 3). The smaller angular coefficient of the Cornell sprinkler (Table 3) than of the double-ring infiltrometer (Table 2) resulted from the difference in the operating limits of the sensors. Errors from fitting the quadratic model to calibrate the surface runoff sensors for the Cornell infiltrometer were also normal, independent and had homogeneous variance (Table 4). The RMSE for calibrating the ring infiltrometer sensors and precipitation and runoff of the Cornell infiltrometer was 0.25 cm, 0.42 cm and 57 mL, respectively, equivalent to 0.25, 0.69 and 0.28 % of the total reading scale.

In the validation stage, the variables determined by the sensors were strongly aligned with the respective variables determined manually (Figures 7 and 8). For example, the angular coefficients of the straight lines of the fitting between manual and automatic reading, as well as the values of the NSE and Willmott indices, were close to 1 (Figures 7 and 8), regardless of the infiltration variable, which indicated high agreement between the infiltration data measured manually and automatically. The Pbias values close to 0 indicate no significant over- or underestimation of the infiltration variables by the proposed automatic in comparison with the manual methodology (Figures 7 and 8). Furthermore, the RMSE between automatic and manual reading of infiltration variables was relatively small, and maybe even negligible hydrologically and for the main implications of measuring

Table 1. Particle size distribution for different horizons of an *Argissolo Vermelho-Amarelo Distrófico abruptico*, where the validation of automated infiltrometers was carried out, Santa Maria/Rio Grande do Sul State, Brazil

Horizon	Layer	Sand			Silt	Clay
		Total	Coarse	Fine		
	m	g kg ⁻¹				
Ap	0.00-0.10	648	239	409	262	90
A1	0.10-0.40	624	230	394	268	108
A2	0.40-0.60	586	176	410	293	121
E	0.60-0.80	604	164	440	341	55
Bt1	0.80-0.90	525	144	381	347	128
Bt2	0.90+	417	128	289	290	293

Particle size distribution determined by pipette method.

infiltration with infiltrometers. For the Cornell infiltrometer methodology, however, errors were slightly greater than for the double ring, perhaps because the errors of the two sensors added up. For example, for a steady infiltration rate, the RMSE in the double ring methodology was 1.53 mm h⁻¹ (Figure 7) and 4.33 mm h⁻¹ by the Cornell methodology (Figure 8). However, it is worth remembering that manual reading is subject to errors. Furthermore, the randomness of errors, regardless of the measurement method (Cornell or double ring) or infiltration variable, shows that the accuracy of the system was not affected by the recorded measurement range (Figures 7 and 8). Automatic systems proposed for double rings, for example, proved to be accurate for points with steady infiltration rates of up to ~270 mm h⁻¹ (Figure 7a). On the other hand, although the linear fitting is within the measurement domain, there is no guarantee that beyond it the relationship will have the same pattern.

Proposed infiltration assessment systems are compact, which ensures practicality in the assessment of water infiltration. Furthermore, automation made it possible to define the infiltration curve clearly, particularly when measured with a double-ring infiltrometer. In the test shown in figure 5, e.g., there were 98 steps of water discharge from the infiltrometer, all of which were subsequently considered as reading intervals of the infiltration curve. In manual measurements, on the other hand, where the time interval between two readings is longer and defined *a priori*, there may not be an exact delimitation of the water discharge points and the resulting infiltration curve may be more irregular. The method also makes it possible to quantify the infiltration that occurs in the first seconds of testing, which is generally impossible with manual readings. This possibly represents an important gain of information for analyzing some factors related to initial infiltration, e.g., antecedent moisture, presence of surface crust, roots, etc. Another positive point of automation, in this case specifically for the Cornell infiltrometer, is that it can determine whether precipitation intensity is constant over time (Figure 6c). In the traditional manual methodology, precipitation intensity is generally assumed to be constant, which is expected based on the principle of Mariotte and if the infiltrometer is well sealed. In this case, measurements of the hydraulic load at the beginning and end of the test would be sufficient to determine the precipitation intensity. However, small air leaks, sometimes unnoticed in the field, can cause the precipitation rate to decrease over time. This can be easily observed in the precipitation sensor data record if the time-recorded measurements show a non-linear trend (Figure 6c).

The systems are easy to build and use pressure transducers and an open-source microcontroller (<https://www.arduino.cc>). This facilitates the measurement of point water infiltration into the soil and enhances the representation of the infiltration curve in relation to manual assessments.

Table 2. Calibration and residues analysis from adjustments of the differential pressure sensors used in the double-ring infiltrometer

Sensor	Ang coef.	p value (F significant)	R ²	RMSE	Normality	Independence	Homoscedasticity
					p valor		
	cm mV ⁻¹			cm			
1	0.0275	2.76E-29	0.999	0.1380	0.4400	0.1700	0.8381
2	0.0273	2.24E-32	0.999	0.1508	0.3240	0.0620	0.1244
3	0.0274	4.91E-26	0.999	0.1449	0.0800	0.8100	0.8275
4	0.0274	3.87E-13	0.999	0.2690	0.7700	0.1580	0.1445
5	0.0274	5.31E-13	0.999	0.2830	0.2750	0.4980	0.8807
6	0.0275	1.25E-11	0.999	0.2210	0.9860	0.5100	0.4692
7	0.0276	1.83E-09	0.999	0.2220	0.1800	0.6800	0.3347
8	0.0275	7.21E-10	0.999	0.1640	0.4690	0.8780	0.1789
9	0.0275	6.94E-11	0.999	0.3140	0.6355	0.8460	0.1900
10	0.0273	1.58E-10	0.999	0.3710	0.8691	0.9020	0.4242

Ang coef.: angular coefficient of linear adjustment; RMSE: root mean squared error.

Table 3. Calibration and residues analysis from adjustment of the differential pressure sensors used in the Cornell infiltrometer to determine precipitation

Sensor	Ang coef.	p value (F significant)	R ²	RMSE	Normality	Independence	Homoscedasticity
					p valor		
	cm mV ⁻¹			cm			
1	0.0161	6.29E-23	0.999	0.2372	0.1803	0.8900	0.5404
2	0.0161	6.15E-17	0.999	0.2455	0.2200	0.4620	0.8240
3	0.0159	3.03E-22	0.999	0.4245	0.8975	0.3940	0.3103
4	0.0160	4.63E-16	0.998	0.6000	0.8189	0.1120	0.2716
5	0.0162	6.47E-17	0.999	0.5100	0.5500	0.7240	0.2738
6	0.0163	7.74E-13	0.999	0.1726	0.5031	0.5880	0.5371
7	0.0160	1.17E-17	0.999	0.4290	0.5031	0.1080	0.4917
8	0.0159	2.58E-23	0.999	0.4280	0.5436	0.4700	0.1291
9	0.0160	8.51E-20	0.999	0.1757	0.0600	0.1480	0.1322
10	0.0161	2.26E-21	0.999	0.3582	0.4496	0.1260	0.1422

Ang coef.: angular coefficient of linear adjustment; RMSE: root mean squared error.

Table 4. Calibration and analysis of residues from adjustments of flow monitoring sensors for Cornell infiltrometer

Sensor	Intersection	coefficients				p value (F significant)	R ²	RMSE	Norm.	Ind.	Hom.
		X	X ²	X ³	X ⁴				p valor		
	mL							mL			
1	26606	-8.7536	-0.0025	3.11E-07	1.08E-10	2.7E-45	0.999	45	0.2836	0.1880	0.4529
2	27808	-11.2153	-0.0010	2.98E-07	-1.25E-11	6.2E-42	0.999	51	0.2388	0.8100	0.1360
3	27699	-11.8176	0.0002	-4.48E-07	1.37E-10	1.8E-40	0.999	45	0.3388	0.4060	0.2436
4	28090	-13.7971	0.0023	-1.30E-06	2.61E-10	8.7E-42	0.999	41	0.3867	0.4940	0.5923
5	26164	-5.2494	-0.0075	3.18E-06	-4.71E-10	2.2E-40	0.999	45	0.0557	0.8080	0.4246
6	28299	-6.0870	-0.0073	3.28E-06	-5.15E-10	5.4E-40	0.999	49	0.0529	0.3620	0.7323
7	29726	-13.6984	0.0012	-5.02E-07	9.55E-11	1.9E-39	0.999	43	0.4002	0.2220	0.2428
8	26092	-1.6994	-0.0110	4.62E-06	-6.85E-10	2.8E-44	0.999	38	0.1499	0.5180	0.3453
9	30026	-17.9559	0.0062	-2.97E-06	5.14E-10	3.1E-37	0.999	83	0.0692	0.9980	0.5594
10	26726	-5.5977	-0.0082	4.27E-06	-7.69E-10	1.5E-38	0.999	73	0.1753	0.1200	0.4628

Norm: Residue normality; Ind: residue independence; Hom: Homoscedasticity; RMSE: root mean squared error.

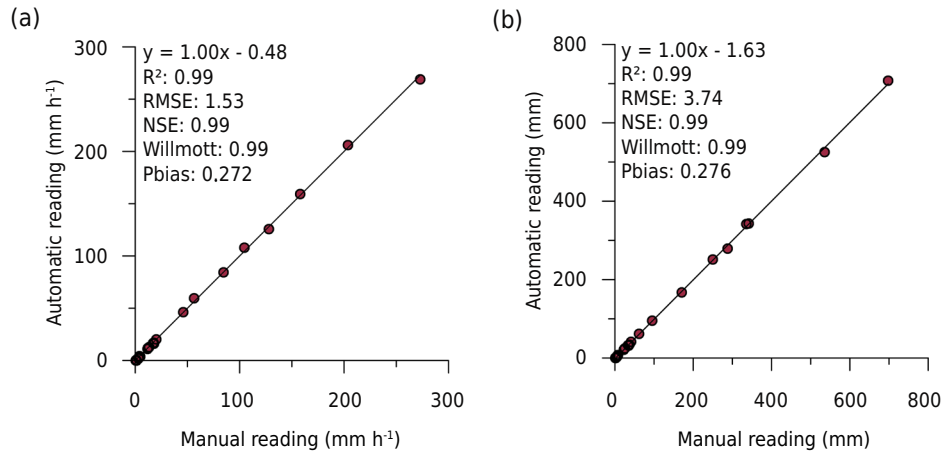


Figure 7. Equipment validation and strategy were used to automatically obtain soil water infiltration variables with a double ring infiltrometer, demonstrating the alignment between manual and automatic reading for steady infiltration rate (a) and cumulative infiltration (b). The equation presented in each variable represents the linear adjustment between manual and automatic reading. RMSE: root mean squared error between manual and automatic reading; NSE: Nash-Sutcliffe model efficiency between manual and automatic reading; Willmott: Willmott agreement index between manual and automatic reading; Pbias: Percent Bias between manual and automatic reading. Black line represents the 1:1 line.

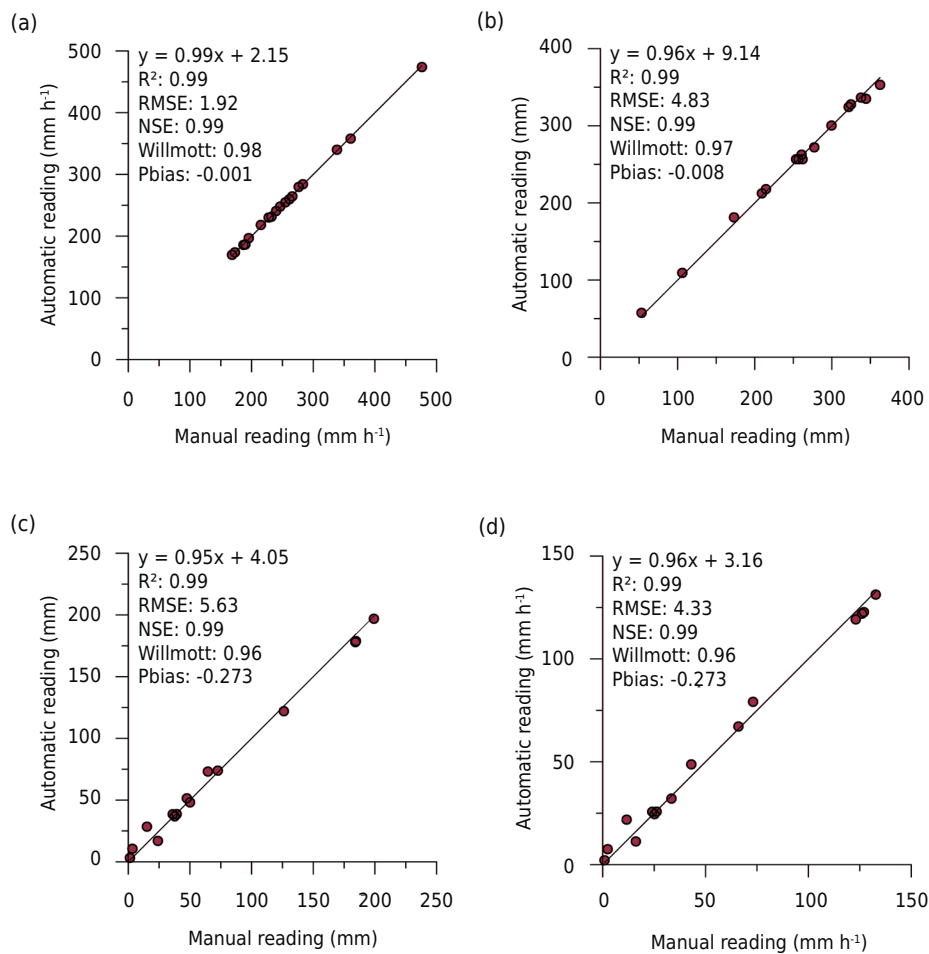


Figure 8. Equipment validation and strategy used to automatically obtain variables of soil water infiltration with a Cornell infiltrometer, demonstrating the alignment between manual and automatic reading for precipitation intensity (a), for cumulative surface runoff (b), for cumulative infiltration (c), and for steady infiltration rate (d). The equation presented in each variable represents the linear adjustment between manual and automatic reading. RMSE: root mean squared error between manual and automatic reading; NSE: Nash-Sutcliffe model efficiency between manual and automatic reading; Willmott: Willmott agreement index between manual and automatic reading; Pbias: Percent Bias between manual and automatic reading. Black line represents the 1:1 line.

CONCLUSIONS

Compact and automated systems were developed and validated for measuring point water infiltration into the soil with concentric-ring and Cornell infiltrometers. Automation with differential pressure sensors monitored with an open-source Arduino microcontroller makes it possible to create point infiltration measurement systems. Systems are not only compact, but also inexpensive and make the recording of the infiltration process and associated variables possible with less operator dependence than manual measurement strategies. Due to the improved resolution resulting from the automation of the infiltrometers, the infiltration curve is better represented, mainly in the initial infiltration phase.

ACKNOWLEDGMENTS

We would like to thank Coordenação de Aperfeiçoamento de Pessoal de Nível Superior (CAPES) – Finance code 001.

AUTHOR CONTRIBUTIONS

Conceptualization:  Dalvan José Reinert (equal),  Fábio Soares Pires (equal),  Lucas Raimundo Rauber (equal),  Micael Stolben Mallman (equal) and  Paulo Ivonir Gubiani (equal).

Data curation:  Lucas Raimundo Rauber (equal) and  Micael Stolben Mallman (equal).

Formal analysis:  Lucas Raimundo Rauber (equal) and  Micael Stolben Mallman (equal).

Investigation:  Francieli de Vargas (equal),  Lucas Raimundo Rauber (equal) and  Micael Stolben Mallman (equal).

Methodology:  Fábio Soares Pires (equal),  Francieli de Vargas (equal),  Lucas Raimundo Rauber (equal) and  Micael Stolben Mallman (equal).

Project administration:  Lucas Raimundo Rauber (lead).

Resources:  Lucas Raimundo Rauber (lead).

Software:  Fábio Soares Pires (equal),  Micael Stolben Mallman (equal) and  Paulo Ivonir Gubiani (equal).

Supervision:  Dalvan José Reinert (lead).

Validation:  Lucas Raimundo Rauber (equal),  Micael Stolben Mallman (equal) and  Paulo Ivonir Gubiani (equal).

Visualization:  Dalvan José Reinert (equal),  Francieli de Vargas (equal),  Lucas Raimundo Rauber (equal),  Micael Stolben Mallman (equal) and  Paulo Ivonir Gubiani (equal).

Writing - original draft:  Lucas Raimundo Rauber (equal) and  Micael Stolben Mallman (equal).

Writing - review & editing:  Dalvan José Reinert (equal),  Fábio Soares Pires (equal),  Francieli de Vargas (equal),  Lucas Raimundo Rauber (equal),  Micael Stolben Mallman (equal) and  Paulo Ivonir Gubiani (equal).

REFERENCES

- Abdelmoneim AA, Daccache A, Khadra R, Bhanot M, Dragonetti G. Internet of things (IoT) for double ring infiltrometer automation. *Comput Electron Agric.* 2021;188:106324. <https://doi.org/10.1016/j.compag.2021.106324>
- Arriaga FJ, Kornecki TS, Balkcom KS, Raper RL. A method for automating data collection from a double-ring infiltrometer under falling head conditions. *Soil Use Manag.* 2010;26:61-7. <https://doi.org/10.1111/j.1475-2743.2009.00249.x>
- Assouline S. Infiltration into soils: Conceptual approaches and solutions. *Water Resour Res.* 2013;49:1755-72. <https://doi.org/10.1002/wrcr.20155>
- Bouwer H. Intake rate: Cylinder infiltrometer. In: Klute A, editor. *Methods of soil analysis. Part 1. Physical and mineralogical methods.* Madison: Soil Science Society of America; 1986. p. 825-44. <https://doi.org/10.2136/sssabookser5.1.2ed.c32>
- Cernicchiaro G, Barmak R, Teixeira WG. Digital interface device for field soil hydraulic conductivity measurement. *J Hydrol.* 2019;576:58-64. <https://doi.org/10.1016/j.jhydrol.2019.06.034>
- Di Prima S. Automated single ring infiltrometer with a low-cost microcontroller circuit. *Comput Electron Agric.* 2015;118:390-5. <https://doi.org/10.1016/j.compag.2015.09.022>
- Di Prima S, Lassabatere L, Bagarello V, Iovino M, Angulo-Jaramillo R. Testing a new automated single ring infiltrometer for Beerkan infiltration experiments. *Geoderma.* 2016;262:20-34. <https://doi.org/10.1016/j.geoderma.2015.08.006>
- Fatehnia M, Paran S, Kish S, Tawfiq K. Automating double ring infiltrometer with an Arduino microcontroller. *Geoderma.* 2016;262:133-9. <https://doi.org/10.1016/j.geoderma.2015.08.022>
- Fundação Estadual de Proteção Ambiental - Fepam. *Diretriz técnica referente ao descarte e ao reúso de efluentes líquidos no âmbito do estado do Rio Grande do Sul.* Porto Alegre: Fepam; 2019.
- Latorre B, Moret-Fernández D, Lyons MN, Palacio S. Smartphone-based tension disc infiltrometer for soil hydraulic characterisation. *J Hydrol.* 2021;600:126551. <https://doi.org/10.1016/j.jhydrol.2021.126551>
- Lewis JD, Amoozegar A, Mclaughlin RA, Heitman JL. Comparison of cornell sprinkle infiltrometer and double-ring infiltrometer methods for measuring steady infiltration Rate. *Soil Sci Soc Am J.* 2021;85:1977-84. <https://doi.org/10.1002/saj2.20322>
- Morbideilli R, Saltalippi C, Flammini A, Govindaraju RS. Role of slope on infiltration: A review. *J Hydrol.* 2018;557:878-86. <https://doi.org/10.1016/j.jhydrol.2018.01.019>
- Moret-Fernández D, González C, Lampurlanés J, Vicente J. An automated disc infiltrometer for infiltration rate measurements using a microflowmeter. *Hydrol Process.* 2012;26:240-5. <https://doi.org/10.1002/hyp.8184>
- Ogden CB, van Es HM, Shindelbeck R. Miniature rain simulator for field measurement of soil infiltration. *Soil Sci Soc Am J.* 1997;61:1041-3. <https://doi.org/10.2136/sssaj1997.03615995006100040008x>
- Rahmati M, Weihermüller L, Vanderborght J, Pachepsky YA, Mao L, Sadeghi SH, et al. Development and analysis of the Soil Water Infiltration Global database. *Earth Syst Sci Data.* 2018;10:1237-63. <https://doi.org/10.5194/essd-10-1237-2018>
- Santos HG, Jacomine PKT, Anjos LHC, Oliveira VA, Lumberras JF, Coelho MR, Almeida JA, Araújo Filho JC, Oliveira JB, Cunha TJF. *Sistema brasileiro de classificação de solos.* 5. ed. rev. ampl. Brasília, DF: Embrapa; 2018.
- Seratto CD, Franchini JC, Seratto FR, Debiassi H, Santos EL, Conte O, Neto SM, Brischiliari V. *Infiltrômetro de aspersão de Cornell aperfeiçoado: aspectos construtivos, operacionais e de manutenção.* Londrina: Embrapa Soja; 2019.
- Soil Survey Staff. *Keys to soil taxonomy.* 12th ed. Washington, DC: United States Department of Agriculture, Natural Resources Conservation Service; 2014.

Somavilla A, Gubiani PI, Zwirtz AL. Tipping bucket prototype for automatic quantification of surface runoff rate in plots. *Rev Bras Cienc Solo*. 2019;43:e0180096. <https://doi.org/10.1590/18069657rbc20180096>

van Es H, Schindelbeck R. Field procedures and data analysis for the cornell sprinkle infiltrometer. Ithaca; Nova Iorque: Cornell University; 2003.